To be published in Applied Optics:

Title:	Error Analysis of Channeled Stokes Polarimeters
Authors:	Luis Gonzalez-Siu,Neil Bruce
Accepted:	24 April 21
Posted	28 April 21
DOI:	https://doi.org/10.1364/AO.423739

Error Analysis of Channeled Stokes Polarimeters

LUIS OSCAR GONZÁLEZ-SIU[1,*] AND NEIL C. BRUCE[1,2]

[1] Instituto de Ciencias Aplicadas y Tecnología, Universidad Nacional Autónoma de México, Circuito Exterior S/N, Ciudad Universitaria, 04510, Mexico City
[2] neil.bruce@icat.unam.mx
[*] Corresponding author: oscargsiu@gmail.com

Compiled April 22, 2021

In this work, an analysis of passive polarimeters with spectral channeling, referred to as Stokes Channeled Spectropolarimeters, is presented. The SCS setup is composed of two thick birefringent retarders followed by a horizontal linear polarizer. The simulation of these polarimeters and two extraction methods for the incident Stokes vector are also presented. The effects of different retarders thickness ratio, the global retardance factor, retardance errors, axes alignment error, and Gaussian noise on RMS errors of the recovered Stokes parameters are presented. Two different, previously published data extraction methods are presented and compared. We find the best polarimeter configurations from the cases studied, and our results suggest a mixed extraction process, using different extraction methods for different Stokes parameters, could give better results reducing the RMS errors by about a factor of five. It is worth mentioning that, even though a calibration procedure is needed to account for the effect of errors, this is out of the scope of this work.

http://dx.doi.org/10.1364/ao.XX.XXXXXX

1. INTRODUCTION

The polarization of light is defined to be the description of the vibration of the electric field [1]. Detectors on their own do not have a strong enough polarization-dependent response, and auxiliary polarization components are required [2]. For this reason many methods have been developed to determine the polarization of light from observable intensities [3–5]. These methods are contained in the field of polarimetry. One of the difficulties of polarimetric measurements is the dependence on temporal resolution, but some methods can work around this. Channeled polarimeters with spatial or spectral channeling have independence from temporal resolution through snapshot polarimetry [2, 6].

Spectroscopic analysis of the state of polarization (SOP) of light plays a major role in polarimetric and ellipsometric studies of dispersive materials [7, 8]. Spectropolarimetry has been widely applied in various application fields, such as remote sensing [9, 10], material characterization [11, 12], and synthesis of novel materials [13–15].

In this paper we study Stokes Channeled Spectropolarimetry (SCS), in particular we study the sensitivity of the extracted Stokes parameters to errors in the experimental setup, to added Gaussian measurement noise, and for two different data extraction schemes. In Section 2 we present the methods to extract the incident Stokes vector. In Section 3 we present the results of various simulations of different configurations and error sources applied. The paper ends with some concluding remarks in Section 4.

2. CHANNELED SPECTROPOLARIMETRY

The fundamental concept of channeled polarimetry can be considered an analog to conventional amplitude modulation [1, 16]. Temporal misregistration, or intensity differences between time-sequential measurements not induced by polarization, can be a significant source of error in certain applications. Such misregistration can be caused by motion of the platform or scene, and is therefore a particular concern in the field of remote sensing [1, 17]. One method that avoids temporal misregistration is referred to as channeled polarimetry, whose techniques make use of polarization interference in order to amplitude modulate the Stokes parameters onto either spectral or spatial carrier frequencies. The use of interference can be beneficial in several respects when compared to a conventional polarimeter. For instance, in a conventional polarimeter, four intensity measurements must be taken (e.g., I_0, I_{90}, I_{135}, and I_R) for the calculation of a complete Stokes vector, where I_R refers to right-circular polarization. Doing so requires these values be manipulated (added and subtracted from one another) within a computer during post processing. Conversely, channeled polarimetry enables the direct measurement of all four Stokes parameters simultaneously, by performing the addition and subtraction optically, through interference between four coherent beams [1]. That is, channeled polarimetry enables snapshot polarimetry [6]. This is feasible because interference maintains the phase of each component within the complex amplitude, before the detector measures the intensity. Consequently, the amplitude and phase of the Stokes parameters are encoded within the amplitude and phase

of the carrier frequency, enabling the magnitude and sign (or handedness) of the Stokes parameters to be extracted [1].

It should be noted that such a cosinusoidally modulated spectrum is generally called a channeled spectrum and is frequently used in the field of frequency-domain interferometry [8]. Each of these harmonic modulations will split the information in the corresponding Fourier domains, creating weighted copies of the Fourier transform of the data at the modulations carrier frequencies. These multiplexed copies are called channels [6].

SCS is often implemented with a spectrometer that uses some form of dispersion, and that must have sufficient wavenumber resolution $\Delta\sigma$ to acquire the fine structure of the channelled spectrum. This implies that smaller wavelength resolution $\Delta\lambda$ is needed for shorter wavelength λ [8].

The SCS configuration of interest is capable of measuring the complete Stokes vector and was proposed by Nordsieck [18], and later studied by Oka and Kato [8], and Iannarilli et al. [19], see Fig. 1. The SCS consists of two thick birefringent retarders, R_1 and R_2, with fast axes orientations at 0° and 45°, respectively; following comes an analyzer, with its transmission axis defining the 0° reference, and the dispersive spectrometer.

The retardance ϕ_i of the thick birefringent retarders is given by $\phi_i = 2\pi\sigma\tau_i$ with $\tau_i = d_0 d_i B$ where σ is the wavenumber; τ_i, the optical path difference (OPD); d_0, the global retardance factor; d_i, the local retardance factor; and B, the birefringence of the retarder. The product $d_0 d_i$ is the retarder's thickness. This means that retardances are linear with wavenumber [2] and that the birefringent plate can serve as a variable retarder when it is combined with a spectroscopic device [8]. In real crystals, the retardance has a more complex dependence with wavenumber.

From Fig. 1, the total Mueller matrix for the SCS is given by

$$\underline{\underline{\mathbf{W}}} = \underline{\underline{\mathbf{M}}}_P(0)\underline{\underline{\mathbf{M}}}_{R2}(\phi_2, \pi/2)\underline{\underline{\mathbf{M}}}_{R1}(\phi_1, 0), \tag{1}$$

where $\underline{\underline{\mathbf{M}}}_P$, $\underline{\underline{\mathbf{M}}}_{R1}$, and $\underline{\underline{\mathbf{M}}}_{R2}$ represent the Mueller matrices of the horizontal linear polarizer and the two birefringent retarders, given by

$$\underline{\underline{\mathbf{M}}}_P(2(0^\circ)) = \frac{1}{2}\begin{pmatrix} 1 & 1 & 0 & 0 \\ 1 & 1 & 0 & 0 \\ 0 & 0 & 0 & 0 \\ 0 & 0 & 0 & 0 \end{pmatrix}, \tag{2}$$

$$\underline{\underline{\mathbf{M}}}_{R1}(\phi_1, 2(0^\circ)) = \begin{pmatrix} 1 & 0 & 0 & 0 \\ 0 & 1 & 0 & 0 \\ 0 & 0 & cos\phi_1 & sin\phi_1 \\ 0 & 0 & -sin\phi_1 & cos\phi_1 \end{pmatrix}, \tag{3}$$

$$\underline{\underline{\mathbf{M}}}_{R2}(\phi_2, 2(45^\circ)) = \begin{pmatrix} 1 & 0 & 0 & 0 \\ 0 & cos\phi_2 & 0 & -sin\phi_2 \\ 0 & 0 & 1 & 0 \\ 0 & sin\phi_2 & 0 & cos\phi_2 \end{pmatrix}. \tag{4}$$

Considering a light source of unknown SOP $\underline{\mathbf{S}}(\sigma)$ and a detector insensitive to polarization, the measured irradiance is given by

$$I(\sigma) = \begin{pmatrix} 1 & 0 & 0 & 0 \end{pmatrix} \underline{\underline{\mathbf{W}}}\,\underline{\mathbf{S}}(\sigma). \tag{5}$$

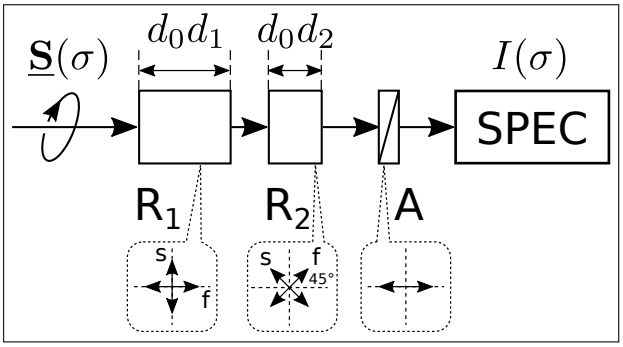

Fig. 1. Stokes channeled spectropolarimeter setup.

Substituting the corresponding matrices yields

$$I(\sigma) = \frac{1}{2}\begin{pmatrix} 1 \\ 0 \\ 0 \\ 0 \end{pmatrix}^T \begin{pmatrix} 1 & C\phi_2 & S\phi_1 S\phi_2 & -C\phi_1 S\phi_2 \\ 1 & C\phi_2 & S\phi_1 S\phi_2 & -C\phi_1 S\phi_2 \\ 0 & 0 & 0 & 0 \\ 0 & 0 & 0 & 0 \end{pmatrix} \begin{pmatrix} S_0(\sigma) \\ S_1(\sigma) \\ S_2(\sigma) \\ S_3(\sigma) \end{pmatrix}, \tag{6}$$

where $C\phi_i = cos(\phi_i)$ and $S\phi_i = sin(\phi_i)$.

This product defines the intensity profile $I(\sigma)$ as a sum of sines and cosines with arguments that are the combinations of different modulations from the system. The intensity spectrum recorded by the detector is given by

$$I(\sigma) = \frac{1}{2}S_0(\sigma) + \frac{1}{2}S_1(\sigma)C\phi_2 + \frac{1}{2}S_2(\sigma)S\phi_1 S\phi_2 - \frac{1}{2}S_3(\sigma)C\phi_1 S\phi_2. \tag{7}$$

From the trigonometric identities of the sine and cosine of the sum of two angles, Eq. (7) is rearranged into

$$\begin{aligned} I(\sigma) =& \frac{1}{2}S_0(\sigma) + \frac{1}{2}S_1(\sigma)C\phi_2 \\ &+ \frac{1}{4}S_2(\sigma)[-C(\phi_1+\phi_2) + C(\phi_1-\phi_2)] \\ &- \frac{1}{4}S_3(\sigma)[S(\phi_1+\phi_2) - S(\phi_1-\phi_2)], \end{aligned} \tag{8}$$

where the effective carrier frequencies of the recorded spectrum are $\tau_i = Bd0di$, i.e. the OPD corresponding to the retardances ϕ_i. Therefore, the carrier frequencies increase with both retarder parameters [1].

The inverse Fourier transform of $I(\sigma)$ gives the autocorrelation function $C(h)$ [8], which describes the modulation channels in the τ-domain (OPD-space) of the spectrum of the SOP we want to know. Using known Fourier transform relations, the autocorrelation function is

$$\begin{aligned} C(h) =& \frac{1}{2}\hat{S}_0(\tau) + \frac{1}{4}\hat{S}_1(\tau) * [\delta(\tau+\tau_2) + \delta(\tau-\tau_2)] \\ &+ \frac{1}{8}\hat{S}_2(\tau) * [-\delta(\tau+\tau_1+\tau_2) - \delta(\tau-\tau_1-\tau_2) \\ &+ \delta(\tau+\tau_1-\tau_2) + \delta(\tau-\tau_1+\tau_2)] \\ &- \jmath\frac{1}{8}\hat{S}_3(\tau) * [\delta(\tau+\tau_1+\tau_2) - \delta(\tau-\tau_1-\tau_2) \\ &- \delta(\tau+\tau_1-\tau_2) + \delta(\tau-\tau_1+\tau_2)], \end{aligned} \tag{9}$$

where δ, with no subscript, is the Dirac delta function, and τ is the Fourier transform variable of σ [1, 2, 6].

Therefore, the channels, $H(\tau-\tau_i)$, can be isolated using a frequency filtering technique [15]. We observe that the autocorrelation function (Eq. (9)) considers six possible modulations (additional channels to the central channel C_0) centred in positions given by

$$\tau = 0, \pm\tau_2, \pm(\tau_1-\tau_2), \pm(\tau_1+\tau_2). \tag{10}$$

Although, we do not expect modulations at $\tau = \pm\tau_1$, we consider it as a reference. Therefore, the autocorrelation function has nine useful modulation channels.

Retardance is a function of the retarder thickness and the wavenumber that passes through the retarder. Nevertheless, as both retarders are made of the same material and are exposed to the same spectrum range, it is considered that the retardances are mainly dependent on the thickness ($d_0 d_i$). Therefore, we propose a classification of the SCS of interest based on the thickness ratio ($d_1 : d_2$) for retarders R_1 and R_2 (see Table 1).

For certain thickness ratios, the number of channels is decreased by means of crosstalk, that is, two or more channels overlap to some extent. When $\phi_1 \neq \phi_2$, we expect six different cases with up to nine channels ($N_C = 9$), see Table 1. It is also noticed that for $\phi_1 = 2\phi_2$ and $\phi_1 = \phi_2/2$, channel $H(\tau \mp (\tau_1-\tau_2))$ is combined (crosstalk) with channel $H(\tau \mp \tau_2)$ and $H(\tau \pm \tau_1)$, respectively. For these cases, the number of channels (N_C) is reduced to seven.

Table 1. Thickness' ratio $(d_1 : d_2)$ classification of SCS

Case	d_1	$(d_1 : d_2)$	Channel relative position				N_C
			τ_1	τ_2	$\tau_1+\tau_2$	$\tau_1-\tau_2$	
1	$< d_2/2$	(1, 3)	1	3	4	-2	9
2	$= d_2/2$	(1, 2)	1	2	3	-1	7
3	$> d_2/2$	(1, 1.5)	2	3	4	-1	9
4	$> 2d_2$	(3, 1)	3	1	4	2	9
5	$= 2d_2$	(2, 1)	2	1	3	1	7
6	$< 2d_2$	(1.5, 1)	3	2	4	1	9

To extract the Stokes vector, two methods were considered: 1) Channel Splitting as described by Oka and Kato [8], and 2) Analytical Channel Splitting as described by Alenin and Tyo [2, 6].

A. Channel Splitting

From the autocorrelation function (Eq. (9)), each channel is isolated using a window filter and applying Fourier analysis we can solve the Stokes parameters [8]. From Eq. (8), the autocorrelation function (Eq. (9)) is rewritten as

$$\begin{aligned} C(h) =& \frac{1}{2}A_0(\tau) + \frac{1}{4}A_1(\tau-\tau_2) + \frac{1}{4}A_1^*(\tau+\tau_2) \\ &+ \frac{1}{8}A_2(\tau-(\tau_1-\tau_2)) + \frac{1}{8}A_2^*(\tau+(\tau_1-\tau_2)) \\ &- \frac{1}{8}A_3(\tau-(\tau_1+\tau_2)) - \frac{1}{8}A_3^*(\tau+(\tau_1+\tau_2)). \end{aligned} \tag{11}$$

The Stokes parameters are obtained using Fourier analysis through the Channel splitting method [8].

$$S_0(\sigma) = \mathcal{F}\{A_0(\tau)\}, \tag{12}$$
$$S_1(\sigma) = \mathcal{F}\{A_1(\tau-\tau_2)\}exp(+\jmath\phi_2), \tag{13}$$
$$S_{23}(\sigma) = \mathcal{F}\{A_3(\tau-(\tau_1+\tau_2))\}exp(+\jmath(\phi_1+\phi_2)), \tag{14}$$
$$= S_2(\sigma) - \jmath S_3(\sigma), \tag{15}$$
$$S_2(\sigma) = Re\{S_{23}\}, \tag{16}$$
$$S_3(\sigma) = Im\{S_{23}\}. \tag{17}$$

We ignore channel $A_2(\tau-(\tau_1-\tau_2))$ because of the crosstalk between channels $H(\tau-(\tau_1-\tau_2))$ and $H(\tau-\tau_2)$, when $\phi_1 = 2\phi_2$. For this case, the autocorrelation function is given by

$$\begin{aligned} C(h) =& \frac{1}{2}\mathcal{F}^{-1}\{S_0(\sigma)\} \\ &+ \frac{1}{4}\mathcal{F}^{-1}\{\Big(S_1(\sigma) + \frac{1}{2}S_{23}(\sigma)\Big)exp(-\jmath\phi_2)\} \\ &+ \frac{1}{4}\mathcal{F}^{-1}\{\Big(S_1(\sigma) + \frac{1}{2}S_{23}^*(\sigma)\Big)exp(+\jmath\phi_2)\} \\ &- \frac{1}{8}\mathcal{F}^{-1}\{S_{23}(\sigma)exp(-\jmath(\phi_1+\phi_2))\} \\ &- \frac{1}{8}\mathcal{F}^{-1}\{S_{23}^*(\sigma)exp(+\jmath(\phi_1+\phi_2))\}. \end{aligned} \tag{18}$$

The Stokes parameters S_0, S_2, and S_3 are still solved using Eq. (12), Eq. (16), and Eq. (17). But the channels with information of S_1 have crosstalk, as stated by Eq. (19).

$$A_1(\tau-\tau_2) = \mathcal{F}^{-1}\{\Big(S_1(\sigma) + \frac{1}{2}S_{23}(\sigma)\Big)exp(-\jmath\phi_2)\}, \tag{19}$$
$$S_1(\sigma) = \mathcal{F}\{A_1(\tau-\tau_2)\}exp(+\jmath\phi_2) - \frac{1}{2}S_{23}(\sigma). \tag{20}$$

B. Analytical Channel Splitting

In order to have an analytical form for the channel splitting method, a construct is needed to recreate the modulations in the Fourier domain. This is obtained through a Frequency Phase Matrix (FPM), which determines the functional form of the modulation and makes Fourier transforms a matter of looking up the correct row of a precalculated matrix [2, 6].

Using the FPM, we obtain a map for each Stokes element splitting, called the $\underline{\underline{\mathbf{Q}}}$-matrix [2]. We say that $\underline{\underline{\mathbf{Q}}}$ maps an input Stokes vector into a channel vector $\underline{\mathbf{C}}$ [6],

$$\underline{\mathbf{C}} = \underline{\underline{\mathbf{Q}}}\,\mathcal{F}^{-1}\{\underline{\mathbf{S}}(\sigma)\}, \tag{21}$$

where $\underline{\mathbf{C}}$ is a matrix formed by concatenating the filtered channels of the autocorrelation function $C(h)$.

From the setup of interest [8, 18], (see Fig. 1), all θ's are forced to be in steps of 45°, which collapses $cos(2\theta)$ and $sin(2\theta)$ to either ±1 or 0. As a result, retardance is the only potential source of modulation [2]. From the autocorrelation function for an ideal SCS (Eq. (9)), we propose a template (see Table 2) for the $\underline{\underline{\mathbf{Q}}}$-matrix based on the local retardance factors d_i. We construct the $\underline{\underline{\mathbf{Q}}}$-matrix by rearranging the rows of the template following the relative positions of the channels, given by the local retardance factors (see Table 1).

The $\underline{\underline{\mathbf{Q}}}$-matrix has a cardinality $[N_C \times M]$ where N_C is the number of channels or modulations, given by the classification proposed in this paper (see Table 1), and M is the number of Stokes parameters ($M = 4$) [2, 6]. To extract the input Stokes vector we need an inverse map, a matrix that indicates which

Table 2. SCS Q-matrix template

Index	OPD	S_0	S_1	S_2	S_3
4	$+\tau_1-\tau_2$			$+1/8$	$-\jmath 1/8$
3	$+\tau_1+\tau_2$			$-1/8$	$+\jmath 1/8$
2	$+\tau_2$		$+1/4$		
1	$+\tau_1$		0		
0	0	$+1/2$			
-1	$-\tau_1$		0		
-2	$-\tau_2$		$+1/4$		
-3	$-\tau_1-\tau_2$			$-1/8$	$-\jmath 1/8$
-4	$-\tau_1+\tau_2$			$+1/8$	$+\jmath 1/8$

channels have to be combined to extract the Stokes vector. That inverse map corresponds to the pseudo-inverse $\underline{\underline{\mathbf{Q}}}^{+}$ [2],

$$\underline{\mathbf{S}}(\sigma)=\underline{\underline{\mathbf{Q}}}^{+}\mathcal{F}\{\underline{\mathbf{C}}\}. \tag{22}$$

It is important to note that a phase shift must be corrected when applying the Fourier transform to the filtered channels. Also, the Stokes parameter S_0 is assumed to vary with wavenumber, both of the methods revised in this work deal with the fluctuations of S_0 inherently as long as the fluctuations are smaller than the effective carrier frequencies of the autocorrelation function.

3. SIMULATIONS, RESULTS, AND DISCUSSION OF SCS CONFIGURATIONS

The general methodology for the SCS simulations is as follows:

1. Select a sample for the incident Stokes vector.
2. Define the SCS configuration, including the spectral range $[\sigma_{min},\sigma_{max}]$, the spectral resolution $\Delta\sigma$, the number of pixels N in the irradiance curve, the nominal global retardance factor, the nominal local retardance factors (thickness ratio), and the sources of error (retardance errors Δd_i, alignment errors ϵ_i, and Gaussian noise amplitude).
3. Run the methods reviewed to simulate the irradiance to be measured.
4. Run the inverse methods to extract the Stokes vector from the irradiance measured, for this purpose consider the irradiance obtained with Eq. (5) with no experimental errors.

Although, it is also true that a calibration procedure is needed to account for the effect of the error sources of interest [15, 20], this work is intended to understand these effects assuming that the SCS works under nominal conditions, that is, without any calibration procedures applied.

For the spectrometer, a σ-wavenumber range from $1.4954\times10^4[cm^{-1}]$ to $1.8408\times10^4[cm^{-1}]$ ($\lambda\sim543-668[nm]$), with a sampling number N of 1024, and a corresponding wavenumber resolution of $(\sigma_{max}-\sigma_{min})/N$ were considered. The sample selected for the results reported is a completely polarized light source with equal energy in each of the Stokes parameters S_1,S_2,S_3: $S=(1,0.577,0.577,0.577)^T$. In this work, a Hann window was applied to the raw data to avoid artifacts in the extracted Stokes parameters [15, 21–23].

To evaluate the performance of the SCS setups of interest, we consider three figures of merit: 1) the root mean square error (RMS) of the extracted elements S_i against their corresponding nominal values $S_{i,nom}$, given by

$$RMS(S_i)=\left[N^{-1}\sum_{j=1}^{N}(S_i-S_{i,nom})_j^2\right]^{1/2}, \tag{23}$$

2) the condition number (CN) of the $\underline{\underline{\mathbf{W}}}$-Mueller matrix and the $\underline{\underline{\mathbf{Q}}}$-matrix of the nominal setup, and 3) the equally weighted variance (EWV) [24] for the same matrices given by Eq. (24)

$$EWV(\underline{\mathbf{A}})=Tr[(\underline{\underline{\mathbf{A}}}^{+})^T\underline{\underline{\mathbf{A}}}^{+}], \tag{24}$$

where $\underline{\underline{\mathbf{A}}}^{+}$ is the pseudo-inverse of $\underline{\underline{\mathbf{A}}}$. In this work, a Stokes parameter is considered immune to an error source if the RMS error is below 0.01

A. Thickness ratio

Six configurations were studied based on the thickness ratio $d_1:d_2$ configurations reviewed (see Table 1), considering a global retardance factor $d_0=13[mm]$ for the birefringent retarders. The high-order retarders were assumed to be made of quartz, and the birefringence was calculated using a model proposed by Ghosh [25]. The retardance shift for the retarders is between 84.68 and $106.10[rad/mm]$ for the wavenumber range.

As expected, the configuration $(2,1)$ presents crosstalk. This affects the figures EWV and CN, compared to the other five configurations (see Fig. 2). Nevertheless, the Stokes vector extraction was similarly acceptable for all six configurations, as shown in Fig. 3. It seems the EWV and the CN are not representative of the SCS perfomance, based on the thickness ratio. For further tests, we decided to focus on the configuration $(3,1)$ ($d_1>2d_2$), which was also used by Oka and Kato [8].

Another figure of merit used in this work is the RMS of the extracted Stokes parameters using the Channel splitting and the Analytical channel splitting methods, see Fig. 4. The RMS provides a better picture of the performance of the SCS for different thickness ratios. To avoid the discrepancies at the edges of the Stokes parameters curves, a consequence of apodization, the RMS was calculated for a reduced wavenumber range from $1.5\times10^4[cm^{-1}]$ to $1.83\times10^4[cm^{-1}]$. It is worth mentioning that, even though it presents crosstalk, the configuration $(2,1)$ had the

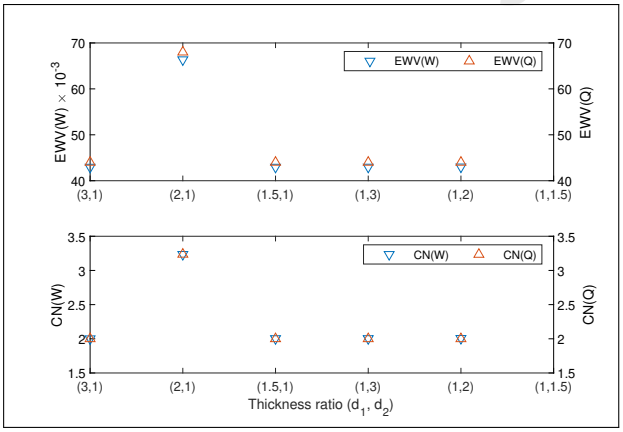

Fig. 2. EWV and CN against the thickness ratio of the SCS.

lowest RMS-scores for S_2 and S_3. This is attributed to channels being tightly packed and uniformly spaced, resulting in the effective separation of the expected channels.

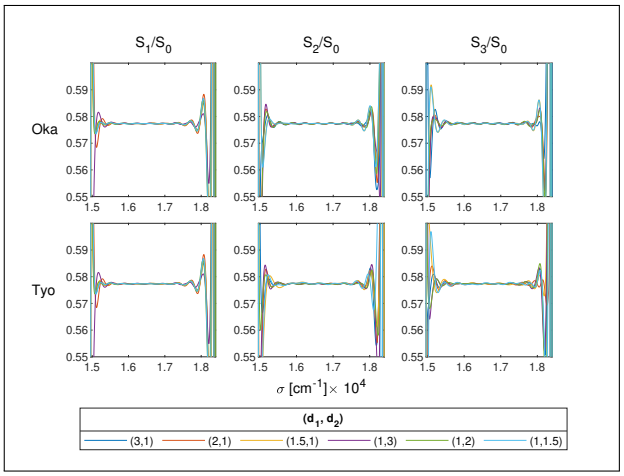

Fig. 3. Normalized Stokes parameters extracted with the Channel splitting and the Analytical channel splitting methods (labeled as Oka and Tyo, respectively). Note that all cases are nearly completely superimposed.

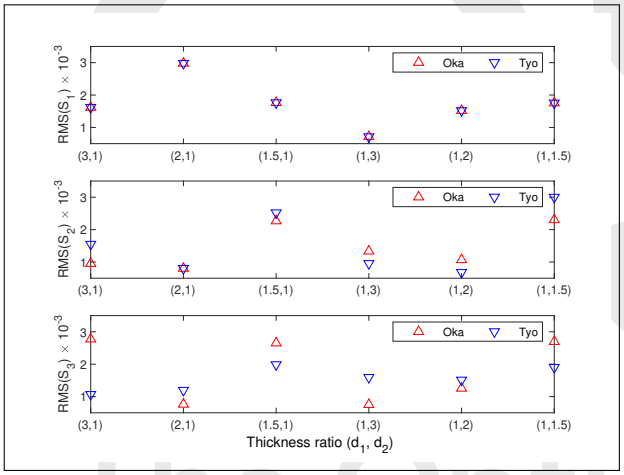

Fig. 4. $RMS(S_i)$ against the thickness ratio of the SCS, for $i = 1, 2, 3$.

B. Global retardance factor

To study the global retardance factor d_0, values from 2 to 40$[mm]$ were considered. In Fig. 5 and 6 are shown the $EWV(W)$ and $CN(W)$ plots, respectively, against d_0. It is observed that the lowest values were obtained for $d_0 = 14, 15[mm]$. However, it is important to note that the input Stokes vector was acceptably extracted for all the d_0-values considered, as shown in Fig. 7.

In Fig. 8 are shown the RMS plots for the Stokes parameters S_1, S_2, and S_3, respectively, for the Channel Splitting and Analytical Channel Splitting methods (labeled as Oka and Tyo, respectively). In general terms, it is also observed that the SCS performance improved as the global retardance factor increased. This is expected, as the separation between channels is directly proportional to d_0, which allows a better filtering process (using the same window, in this work a window of 20 pixels in the

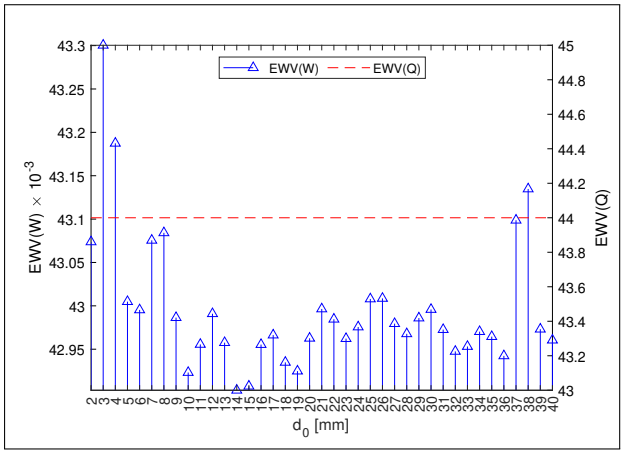

Fig. 5. EWV against the global retardance factor $d_0 = 2 - 40[mm]$.

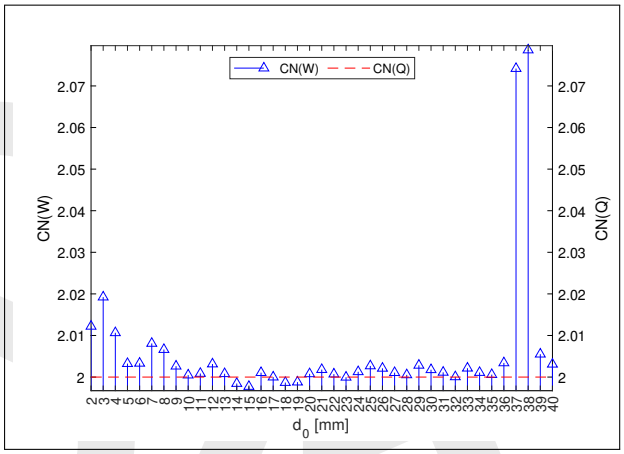

Fig. 6. CN against the global retardance factor $d_0 = 2 - 40[mm]$.

τ-domain was considered). The performance for small values of d_0 could be improved by analysing the window width parameter for each d_0-value. Sabatke *et al.* [21] suggest a window filter with a bandwidth equal to the OPD of the thinner retarder (Bd), but this was not tested in this work. It is considered that $d_0 = 17[mm]$ offered the best performance overall, comparing the RMS plots for the three Stokes parameters.

C. Retardance error

Because of the manufacturing tolerance, the thickness of high-order retarders may deviate from theoretical values, causing the retardations to change [15]. Therefore, a fabrication tolerance Δd_i of $\pm 5[\mu m]$ was considered and it was assumed that the plates had completely flat and parallel faces. The fabrication tolerance was taken from manufacturers tolerances offered for custom thick birefringent quartz plates.

Three global retardance factors were considered: 1) $13[mm]$, value reported in a literature example [8], 2) $14[mm]$, the value with the lowest $EWV(\underline{\mathbf{W}})$ see Fig. 5, and 3) $17[mm]$, the global retardance factor which was considered to offer the best performance overall, see Fig. 8. The thickness ratio considered from this test forward was $(3, 1)$. The retardance error cause a lateral displacement of the channels in the τ-domain, because the OPD is directly proportional to the retardance.

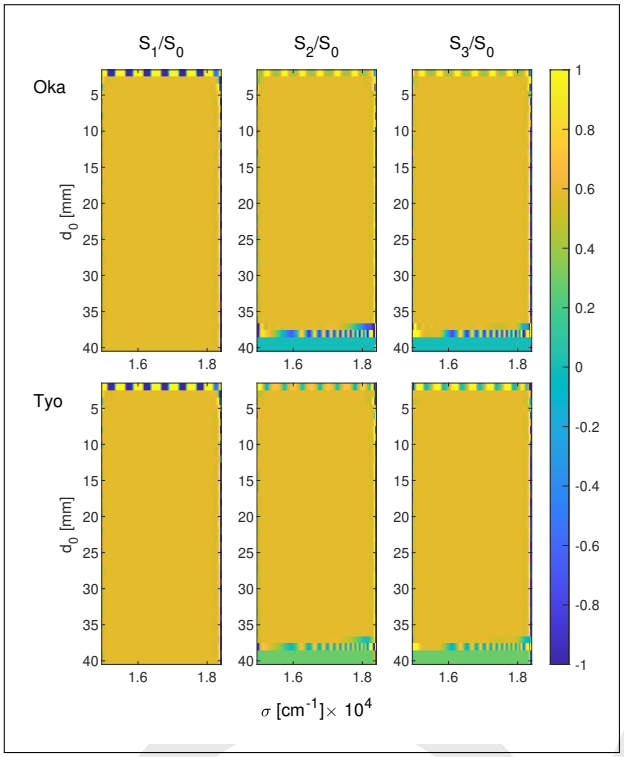

Fig. 7. Normalized Stokes parameters against the global retardance factor $d_0 = 2 - 40[mm]$.

In Fig. 9 are shown the $RMS(S_i)$ plots for the Channel Splitting and Analytical Channel Splitting methods (labeled as Oka and Tyo, respectively) when the retardance error occurs in the first retarder. It is observed that S_1 is immune to the retardance error, whereas, on the contrary, S_2 and S_3 are very sensitive to this error source.

In Fig. 10 are shown the $RMS(S_i)$ plots when the retardance error occurs in the second retarder. It is observed that S_1 is acceptably extracted, but it is not immune. For S_2 and S_3, the Analytical Channel Splitting method achieved a good performance, near to immunity, whereas the Channel Splitting method is highly sensitive to the error source.

D. Alignment error

The assembly process of an instrument is not perfect; therefore, the alignment errors (ϵ_i) of high-order retarders are unavoidable [15]. An alignment tolerance of ± 5 degrees was considered for the retarders. In Fig. 11 are shown the $RMS(S_i)$ plots when the alignment error occurs in the first retarder which has a nominal orientation of $\theta_1 = 0°$. S_1 is very sensitive to the alignment error. For S_2, the Channel Splitting method offers acceptable results, but not immunity to the error source, whereas the Analytical Channel Splitting method is very sensitive to it in the simulation. S_3 is very sensitive when applying the Channel Splitting method, but it is immune when the Analytical Channel Splitting method is applied.

In Fig. 12 are shown the $RMS(S_i)$ plots when the alignment error occurs in the second retarder which has a nominal orientation of $\theta_2 = 45°$. It is observed that S_1 is immune to the error source. When the Analytical Channel Splitting method is used, S_2 and S_3 are also immune.

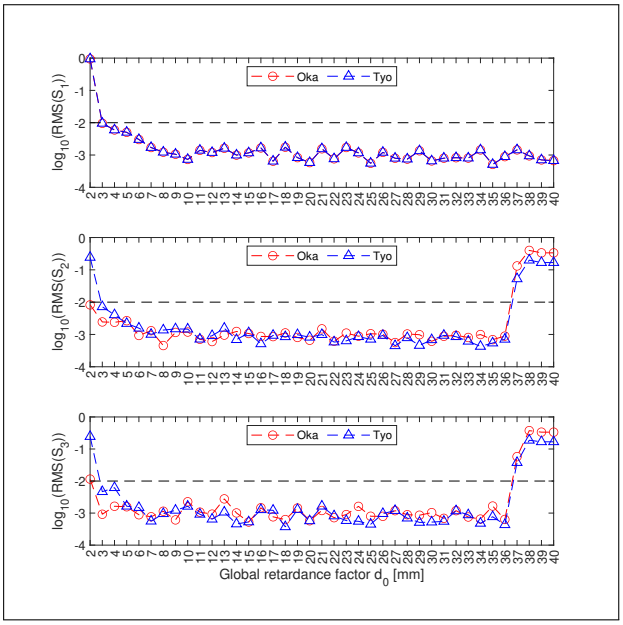

Fig. 8. $RMS(S_i)$ against the global retardance factor of the SCS, for $i = 1, 2, 3$.

E. Gaussian noise

A random Gaussian noise distribution was added to the spectrum leaving the SCS before entering the spectrometer. The amplitudes considered ranged from $1E-6[a.u]$ to $1E0[a.u]$, including a reference without noise. It is observed that a signal-to-noise ratio (SNR) of $10:1$ is acceptable, but a total RMS error of less than 0.01 is achieved for SNR greater or equal to $100:1$, see the $RMS(S_i)$ plots in Fig. 13. This SNR requirement is achievable with commercially available spectrometers. In this work, the SNR is defined by the relation between the unitary amplitude of the normalized irradiance spectrum and the order of magnitude of the added noise amplitude.

4. CONCLUSION

In this paper, the results of analysis and simulations regarding passive channeled polarimeters, specifically with spectral channeling, were presented. Two extraction methods were also described, analysed and compared. Two figures of merit, equally weighted variance (EWV) and condition number (CN), were studied to find their relevance in the polarimeter performance and noise immunity. The main metric to evaluate the performance of the polarimeter was the root mean square error (RMS). It was found that the EWV and the CN are not good metrics to describe the behaviour of the different polarimeter configurations.

Overall, the parameter S_1 was extracted with better results than S_2 and S_3, with similar results for the two extraction methods used, although, to achieve an acceptable extraction, S_1 requires a tolerance of $\pm 1[°]$ for the alignment error of the first retarder. The extraction of the parameters S_2 and S_3 is more sensitive to the error sources studied. Interestingly, they tend to present a mirrored behaviour when comparing the results of the channel splitting and the analytical channel splitting methods. For example, for some global retardance factors reviewed, when the channel splitting method has a better performance for S_2, the analytical channel splitting method works better for S_3. For

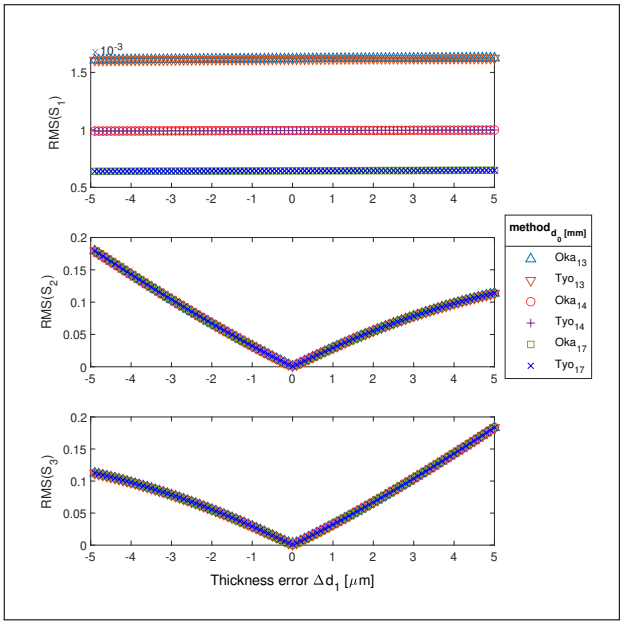

Fig. 9. $RMS(S_i)$ against the thickness error Δd_1, for $i = 1, 2, 3$, in the first retarder with a nominal thickness $3d_0$.

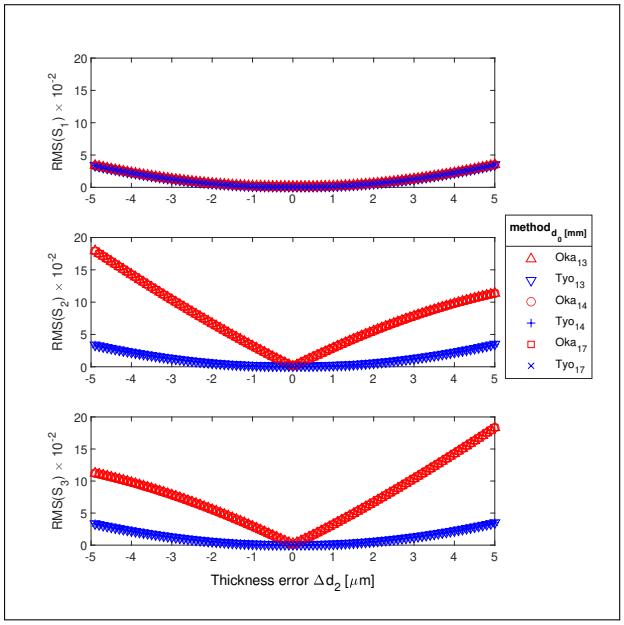

Fig. 10. $RMS(S_i)$ against the thickness error Δd_2, for $i = 1, 2, 3$, in the second retarder with a nominal thickness $d0$.

most of the other factors, the opposite behaviour was observed. This presents an opportunity to develop a mixed extraction technique using both methods to increase the overall immunity of the SCS to certain error sources.

Although, the configuration $(2, 1)$ has the highest EWV and CN values due to the overlapping of two pairs of channels, all six configurations studied allowed the extraction of the Stokes parameters within the immunity condition. Furthermore, the configuration $(2, 1)$ achieved the lowest RMS values for the parameters S_2 and S_3. This is attributed to the information being packed in fewer channels, leading to a lower probability of crosstalk, and to the analytical development of the specific model of this configuration. The best configurations to extract the parameters S_1, S_2, S_3 were $(1, 3), (2, 1), (2, 1)$, respectively.

The global retardance factor has to be greater than $5[mm]$, it was observed that the performance of the SCS improved with this condition. This is at least considering the current algorithm implemented for the automatic channel detection and filtering process. Nevertheless, as this factor is directly related to the channel distribution, the number of pixels and the spectrometer spectral range have to be modified in accordance to optimize the distribution of channels in the autocorrelation function, in order to avoid crosstalk around the DC channel (C_0).

Funding. Dirección General de Asuntos del Personal Académico - Universidad Nacional Autónoma de México (PAPIIT-DGAPA, UNAM) (IT100417 and IG100121).

Acknowledgments. Luis Oscar González-Siu acknowledges a grant provided under the Programa Nacional de Posgrados de Calidad (PNPC) of Consejo Nacional de Ciencia y Tecnología (CONACYT) and Programa de Maestría y Doctorado en Ingeniería (PMDI) from the National Autonomous University of Mexico (UNAM).

Disclosures. The authors declare no conflict of interest.

Data Availability Statement. Data underlying the results presented in this paper are not publicly available at this time but may be obtained from the authors upon reasonable request.

REFERENCES

1. D. Goldstein, *Polarized Light* (CRC Press, New York, 2011), 3rd ed.
2. A. S. Alenin and J. S. Tyo, "Task-specific snapshot Mueller matrix channeled spectropolarimeter optimization," in *Polarization: Measurement, Analysis, and Remote Sensing X,* vol. 8364 (2012), pp. 836402–836402–13.
3. R. M. A. Azzam, "Photopolarimetric measurement of the Mueller matrix by Fourier analysis of a single detected signal," Opt. Lett. **2**, 148 (1978).
4. D. B. Chenault, J. L. Pezzaniti, and R. A. Chipman, "Mueller matrix algorithms," in *Polarization Analysis and Measurement,* vol. 1746 D. H. Goldstein and R. A. Chipman, eds. (1992), pp. 231–246.
5. D. B. Chenault, "Spectropolarimetric reflectometer," Opt. Eng. **41**, 1013 (2002).
6. A. S. Alenin and J. S. Tyo, "Generalized channeled polarimetry," J. Opt. Soc. Am. A **31**, 1013 (2014).
7. D. E. Aspnes, "Analysis Of Semiconductor Materials And Structures By Spectroellipsometry," in *Spectroscopic Characterization Techniques for Semiconductor Technology III,* vol. 0946 O. J. Glembocki, F. H. Pollak, and F. A. Ponce, eds. (1988), p. 84.
8. K. Oka and T. Kato, "Spectroscopic polarimetry with a channeled spectrum," Opt. Lett. **24**, 1475 (1999).
9. D. J. Diner, R. A. Chipman, N. A. Beaudry, B. Cairns, L. D. Foo, S. A. Macenka, T. J. Cunningham, S. Seshadri, and C. U. Keller, "An integrated multiangle, multispectral, and polarimetric imaging concept for aerosol remote sensing from space," in *Enabling Sensor and Platform Technologies for Spaceborne Remote Sensing,* vol. 5659 G. J. Komar, J. Wang, and T. Kimura, eds. (2005), p. 88.
10. S. H. Jones, F. J. Iannarilli, C. Hostetler, B. Cairns, A. Cook, J. Hair, D. Harper, Y. Hu, and D. Flittner, "Preliminary airborne measurement results from the Hyperspectral Polarimeter for Aerosol Retrievals (HySPAR)." NASA Earth Sci. Technol. Conf. Proc. pp. 1–6 (2006).
11. N. Gupta and D. R. Suhre, "Acousto-optic tunable filter imaging spectrometer with full Stokes polarimetric capability," Appl. Opt. **46**, 2632 (2007).
12. N. Gupta, "Acousto-optic tunable filter based spectropolarimetric imagers," in *Polarization: Measurement, Analysis, and Remote Sensing VIII,* vol. 6972 D. B. Chenault and D. H. Goldstein, eds., International Society for Optics and Photonics (SPIE, 2008), pp. 88–98.
13. B. P. Cumming, G. E. Schröder-Turk, S. Debbarma, and M. Gu, "Bragg-mirror-like circular dichroism in bio-inspired quadruple-gyroid 4srs

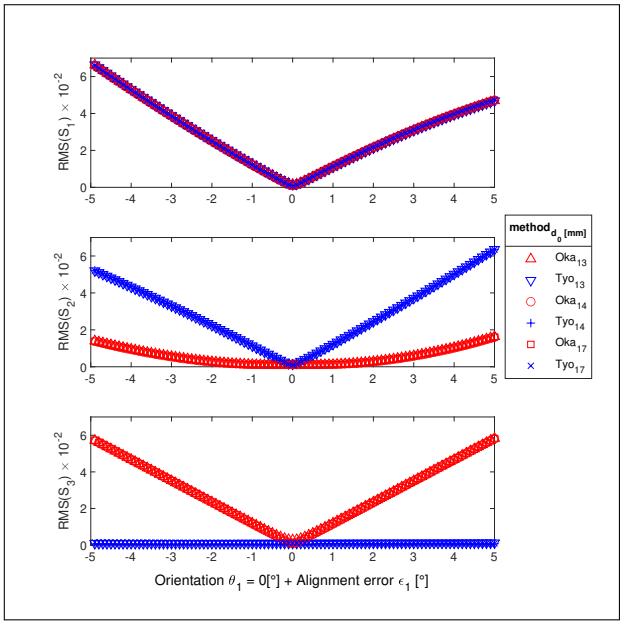

Fig. 11. $RMS(S_i)$ against the alignment error ϵ_1, in the first retarder with a nominal orientation of $\theta_1 = 0°$.

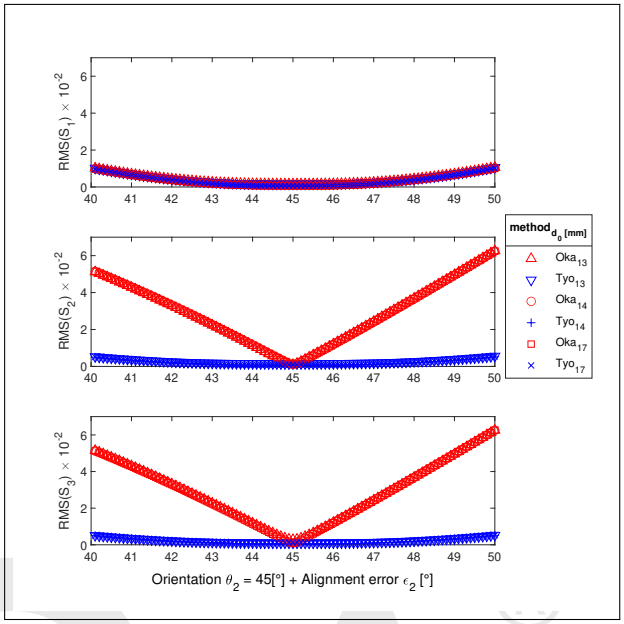

Fig. 12. $RMS(S_i)$ against the alignment error ϵ_2, for $i = 1, 2, 3$, in the second retarder with a nominal orientation of $\theta_2 = 45°$.

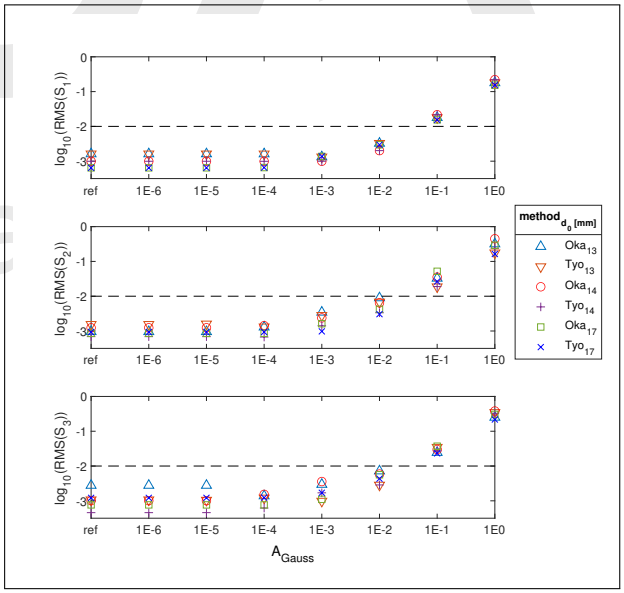

Fig. 13. $log_{10}(RMS(S_i))$ against the Gaussian noise distribution amplitude, for $i = 1, 2, 3$.

nanostructures," Light. Sci. Appl. **6**, 1–8 (2017).
14. A. Y. Zhu, W. T. Chen, A. Zaidi, Y. W. Huang, M. Khorasaninejad, V. Sanjeev, C. W. Qiu, and F. Capasso, "Giant intrinsic chiro-optical activity in planar dielectric nanostructures," Light. Sci. Appl. **7**, 17158 (2018).
15. X. Ju, B. Yang, C. Yan, J. Zhang, and W. Xing, "Easily implemented approach for the calibration of alignment and retardation errors in a channeled spectropolarimeter," Appl. Opt. **57**, 8600 (2018).
16. D. S. Sabatke, A. M. Locke, R. W. McMillan, and E. L. Dereniak, "Linear operator theory of channeled spectropolarimetry," J. Opt. Soc. Am. A **22**, 1567 (2005).
17. J. S. Tyo, D. L. Goldstein, D. B. Chenault, and J. A. Shaw, "Review of passive imaging polarimetry for remote sensing applications," Appl. Opt. **45**, 5453 (2006).
18. K. H. Nordsieck, "A Simple Polarimetric System for the Lick Observatory Image-Tube Scanner," Publ. Astron. Soc. Pac. **86**, 324 (1974).
19. F. J. Iannarilli, Jr., S. H. Jones, H. E. Scott, and P. L. Kebabian, "Polarimetric-spectral intensity modulation (P-SIM): enabling simultaneous hyperspectral and polarimetric imaging," in *Infrared Technology and Applications XXV,* vol. 3698 B. F. Andresen and M. Strojnik, eds. (1999), p. 474.
20. A. Taniguchi, K. Oka, H. Okabe, and M. Hayakawa, "Stabilization of a channeled spectropolarimeter by self-calibration," Opt. Lett. **31**, 3279 (2006).
21. D. S. Sabatke, A. M. Locke, E. L. Dereniak, and R. W. McMillan, "Linear calibration and reconstruction techniques for channeled spectropolarimetry," Opt. Express **11**, 2940 (2003).
22. M. Takeda, H. Ina, and S. Kobayashi, "Fourier-transform method of fringe-pattern analysis for computer-based topography and interferometry," J. Opt. Soc. Am. **72**, 156 (1982).
23. F. Harris, "On the use of windows for harmonic analysis with the discrete Fourier transform," Proc. IEEE **66**, 51–83 (1978).
24. D. S. Sabatke, M. R. Descour, E. L. Dereniak, W. C. Sweatt, S. A. Kemme, and G. S. Phipps, "Optimization of retardance for a complete Stokes polarimeter," Opt. Lett. **25**, 802 (2000).
25. G. Ghosh, "Dispersion-equation coefficients for the refractive index and birefringence of calcite and quartz crystals," Opt. Commun. **163**, 95–102 (1999).